

# Data-Free Group-Wise Fully Quantized Winograd Convolution via Learnable Scales

Shuokai Pan

Gerti Tuzi

Sudarshan Sreeram

Dibakar Gope

Arm Inc.

{shuokai.pan, dibakar.gope}@arm.com

## Abstract

*Despite the revolutionary breakthroughs of large-scale text-to-image diffusion models for complex vision and downstream tasks, their extremely high computational and storage costs limit their usability. Quantization of diffusion models has been explored in recent works to reduce compute costs and memory bandwidth usage. To further improve inference time, fast convolution algorithms such as Winograd can be used for convolution layers, which account for a significant portion of computations in diffusion models. However, the significant quality loss of fully quantized Winograd using existing coarser-grained post-training quantization methods, combined with the complexity and cost of finetuning the Winograd transformation matrices for such large models to recover quality, makes them unsuitable for large-scale foundation models. Motivated by the presence of a large range of values in them, we investigate the impact of finer-grained group-wise quantization in quantizing diffusion models. While group-wise quantization can largely handle the fully quantized Winograd convolution, it struggles to deal with the large distribution imbalance in a sizable portion of the Winograd domain computation. To reduce range differences in the Winograd domain, we propose finetuning only the scale parameters of the Winograd transform matrices without using any domain-specific training data. Because our method does not depend on any training data, the generalization performance of quantized diffusion models is safely guaranteed. For text-to-image generation task, the 8-bit fully-quantized diffusion model with Winograd provides near-lossless quality (FID and CLIP scores) in comparison to the full-precision model. This, coupled with the development of highly optimized kernels for group-wise fully quantized Winograd, improves CPU wall-clock time by 31.3% when compared to the convolution layers of a diffusion model. For image classification, our method outperforms the state-of-the-art Winograd PTQ method by 1.62% and 2.56% in top-1 ImageNet accuracy on ResNet-18 and ResNet-34, respectively, with Winograd F(6, 3).*

## 1. Introduction

In recent years, foundational pre-trained diffusion models have gained a rapid rise in popularity in the field of image generation due to their ability to produce complex and incredibly detailed high-quality photorealistic images from natural language prompts [28, 30, 31, 35]. Furthermore, foundation DMs have successfully demonstrated their flexibility in supporting and achieving high-quality performance on a wide range of downstream computer vision tasks, such as image edition, style transformation, image super-resolution, image-to-image translation, and many others, in contrast to previous Generative Adversarial Networks-based image generation models that suffered from unstable training [9]. However, diffusion models typically require many denoising steps and forward passes to convert Gaussian noises into real images using neural network layers with over 1 billion parameters. Therefore, deploying these large-scale diffusion models to on-device for inference has been a significant challenge due to their unprecedented size, memory bandwidth, and compute cost requirements [38].

Quantization has proven to be an effective method for converting high-precision (16 or 32-bit) model weights and activations to lower-precision values, such as 8-bit integers, reducing the model’s memory and computational requirements while maintaining accuracy, making it more suitable for deployment on devices with limited resources. Among different quantization methods, data-free post-training quantization (PTQ) compresses model parameters after training. While previous studies attempted to quantize weights and activations in diffusion models using coarse-grained PTQ techniques [4, 12, 17, 33, 39, 42, 43, 46], such as tensor-wise or channel-wise quantization, they often resulted in tangible loss of quality, especially under low-bit settings. One issue with these coarser-grained quantization approaches is that outlier values, i.e., outliers, can have a disproportionate impact on scaling: the full range of the lower-precision data type is not used effectively, which lowers the quantized model’s accuracy. Finer-grained group-wise quantization instead has shown great promise in suc-

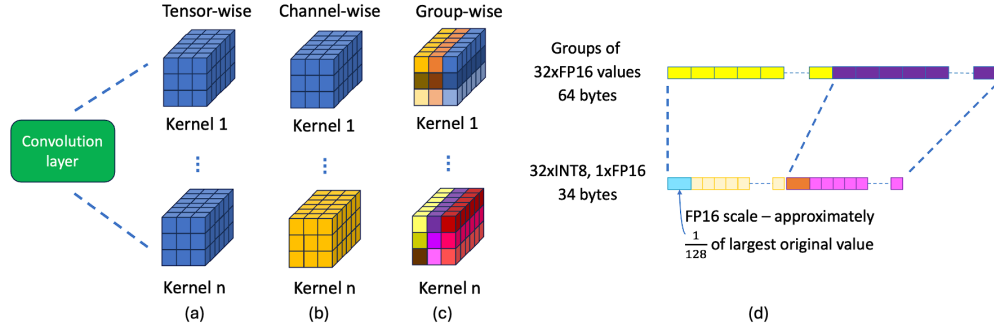


Figure 1. Group-wise quantization for convolution layers.

cessfully quantizing and compressing large-scale generative AI foundation models, particularly large language models. Group-wise quantization [7] has a finer granularity than standard tensor-wise or channel-wise quantization, allowing it to reduce quantization noise natively while approaching the high-precision (floating point) quality of a foundation model. Group-wise quantization quantizes in groups, whereby weights are divided into groups of 32, 64, or 256. Each group is then quantized individually to mitigate the effect of outliers and increase precision.

In this work, in an attempt to preserve image generation quality, we investigate the impact of group-wise quantization of weights and activations in large-scale diffusion models while ensuring high runtime performance through the development of highly optimized matrix multiply kernels for group-wise quantized diffusion models.

While group-wise quantization accelerates inference, the high computational costs of these large-scale foundation models necessitate further speedups to meet response time requirements and pave the way for the deployment of them on edge or mobile devices. Convolution operations account for a significant fraction of the computation time in large-scale diffusion models during inference and training. Different algorithmic methods have been devised to speed up this core operation. Among other compression techniques for reducing this cost, fast convolution algorithms in replacement of direct convolutions, such as Winograd convolution algorithms [15], are observed to accelerate the widely used small-size convolution and can provide additional speedups. While Winograd convolution computation in the quantized domain can significantly accelerate diffusion models, its use in the quantized context results in a significant increase in quantization noise and a subsequent drop in quality, as observed in previous studies [5, 6, 10, 25]. The use of group-wise quantization can largely resolve the quantization and associated numerical error problem of input transformation and element-wise multiplications in the Winograd domain. However, it cannot quantize the intermediate values for output transformation, which account for a significant portion of the com-

pute time, in the Winograd domain well due to the large range differences in values, which can result in a significant degradation in quality when applying group-wise quantization to Winograd convolutions. Previous studies either used costly learning of the Winograd transformation matrices to recover network accuracy [10] or performed quantization-aware training or finetuning of the Winograd matrices with a domain-specific dataset [5], which could lead to overfitting. They may not perform well on previously unseen datasets, particularly for foundation models and various downstream tasks in the production setting. QAT can cause overfitting to small training data sets, so it is generally not recommended for foundational models to maintain their pristine quality.

In this work, we show that the small set of scale factors associated with Vandermonde matrices that derive the Winograd transformation matrices can only be altered to limit the large distribution imbalance of intermediate values in the Winograd domain. Furthermore, these scale factors can be finetuned using random noise without the need for any domain-specific dataset. We derive this requirement from a theoretically grounded analysis. The generalization ability of our data-free group-wise quantized Winograd is inherently guaranteed since it does not need any input data.

The key contributions of this work are as follows:

- We propose a novel hardware-aware quantized Winograd convolution algorithm that uses group-wise quantization to fully quantize all Winograd pipeline operations. To the best of our knowledge, this is the first empirical demonstration of quantized Winograd convolution’s impact on large-scale image generation models.
- We propose fine-tuning only the scale parameters of the Winograd transformation to reduce dynamic range differences. Data-free finetuning makes things transferable to other datasets, which is a prerequisite for foundational models. To the best of our knowledge, we are the first to perform full quantization of Winograd convolution with large tile sizes and ensure high quality without using any training or calibration data.
- We restrict the group size to be either an integer multiple or at least equal to a processor’s vector width to bene-

fit from vectorization. Our group-wise quantized matrix multiply kernels for Winograd convolution, developed as part of this work, can take advantage of the efficient vectorized matrix multiply operations in a processor, significantly improving the runtime performance of convolution and transformer layer operations.

- Our group-wise 8-bit fully quantized diffusion models with Winograd convolutions in conjunction with learned scales provide comparable image generation performance (very small FID change). It also demonstrates superior classification accuracy (2.56% improvement in accuracy for the ImageNet dataset on ResNet34) when compared to state-of-the-art approaches, while optimized kernels ensure a 31.3% improvement in runtime performance over standard convolutions (12.8% improvement for end-to-end diffusion models).

## 2. Related work

**Diffusion models.** Diffusion models [31] can produce high-quality images using an iterative denoising process. They primarily consist of a text encoder, a denoising neural network, such as UNet, in which the convolution layers can take up a significant portion of the time, and an image decoder. Although denoising diffusion models have demonstrated phenomenal capabilities in a range of generative tasks, their slow generation speed prevents their widespread deployment. This can be attributed to their lengthy iterative denoising process through the UNet and high computational demand of the UNet at each step. While numerous studies have been conducted to accelerate this sampling process [21, 24, 32, 45] and design fast samplers [22, 35, 36], in this work we investigate model quantization on diffusion models, which is an orthogonal direction to the above methods and can significantly reduce the computational complexity of the denoising network at each sampling step, thereby further accelerating the sampling process.

**Diffusion model quantization.** Model quantization can be categorized into two types: quantization-aware training (QAT) and post-training quantization (PTQ). QAT often has negligible impacts on model quality after quantization. However, this requires the original training pipeline and datasets, which can be very challenging to set up, especially for large-scale generative AI foundation models. PTQ, on the other hand, applies model quantization after training and usually only requires a small number of samples for calibration of the quantization parameters. Hence, it is much less time-consuming and computationally intensive, generally more favored in network deployment, and is the focus of this work. However, PTQ can lead to significant model quality degradation if not applied carefully. Many PTQ methods have thus been proposed to tackle this issue, for instance, by minimizing the reconstruction errors of tensors before and after quantization [18, 27]. The uni-

form quantization of a floating-point tensor  $x$  into  $b$ -bit integer can be written as,

$$x_{int} = \text{clamp}\left(\left\lfloor \frac{x}{s} \right\rfloor, c_{min}, c_{max}\right)$$

$$x \approx s * x_{int} = \hat{x} \quad (1)$$

PTQ of diffusion models has been studied in a number of previous works [4, 12, 17, 33, 34, 39, 40, 42, 43, 46]. One of the key observations is that the activation distributions of the noise estimation network change greatly over the sampling time steps [17]. [43] emphasizes the importance of activation outliers. Thus, advanced calibration processes have been proposed in these works, but they can be quite complicated and are not easily transferable from one architecture to another [4]. In this work, we proposed to tackle this problem with the more flexible group-wise quantization, which is inherently more robust to distribution changes because the activation quantization parameters are computed for each group of values and dynamically.

**Quantized Winograd convolution.** Winograd algorithms [15] are fast convolution algorithms based on minimal filtering theory [44], and they are well-known for being the fastest implementation of small convolution kernels found in modern neural networks. The Winograd algorithm, similar to the FFT, converts tiles of input activations and weight elements into the Winograd domain before performing element-wise multiplications or Hadamard product, which reduces theoretical computation complexity, as shown in Figure 2. In general, the larger the tile size, the greater the reduction in computational complexity. However, this is not always preferred because larger tile sizes result in greater numerical errors due to the exponentially increasing values of the Winograd transformation matrices as tile size increases. This is also the main reason why Winograd algorithms are typically implemented using 32-bit floating-point arithmetic and with relatively small tile sizes, such as  $4 \times 4$ .

Previous studies [5, 6, 10, 16, 25] have investigated combining Winograd convolution with quantization; however, some [16] only quantized the Hadamard multiplication while doing the input and output transformations in floating-point arithmetic. [10] proposes a flexible Winograd convolution scheme by treating the transformation matrices as learnable parameters. However, this requires a full training pipeline setup, similar to the complexity of QAT. Instead of expensive QAT, [5] performs a two-stage finetuning process to finetune the Winograd transformation matrices with a small set of training samples. However, it cannot fully restore full-precision model accuracy for larger Winograd  $F(6, 3)$ . Our work nearly bridges the accuracy gap with the full-precision model while fully quantizing Winograd convolution without requiring any training samples or domain-specific data.

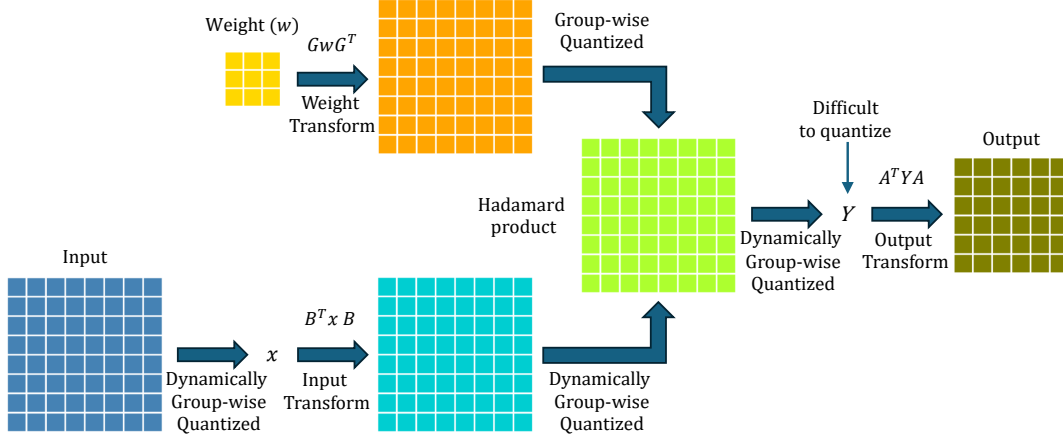


Figure 2. Group-wise fully quantized Winograd convolution. Applying group-wise quantization to Hadamard product and input transformation has a minimal impact on model quality. However, doing the same with the output transformation leads to a significant drop in model accuracy. Weight transformation can be done offline with high precision.

### 3. Group-wise fully quantized Winograd convolution

#### 3.1. Winograd convolution

Using Winograd, the computation of a 2D convolution output tile,  $y$ , of size  $m \times m$  with a kernel filter of size  $r \times r$ , as presented in [15] as  $F(m \times m, r \times r)$ , is often given by,

$$y = A^T \left[ [GwG^T] \odot [B^T xB] \right] A \quad (2)$$

or in more details,

$$W = GwG^T \quad (3)$$

$$X = B^T xB \quad (4)$$

$$Y = W \odot X \quad (5)$$

$$y = A^T Y A \quad (6)$$

where  $w$  is a  $r \times r$  filter, and  $x$  is an  $(m + r - 1) \times (m + r - 1)$  input tile.  $B$ ,  $G$ , and  $A$  are called Winograd transformation matrices, where  $B$  and  $G$  transform the weights and input feature maps, respectively, from the spatial domain to the Winograd domain, and  $A$  transforms the output feature maps ( $Y$ ) back to the spatial domain, after the element-wise multiplication denoted by  $\odot$ . This is also often short-handed to  $F(m, r)$  when the tile and filter are square matrices, which is used in this work.

The Winograd transformation matrices can be constructed from the Chinese remainder theorem by choosing  $n = m + r - 1$  pairs of so-called polynomial points or Lagrange interpolation points  $(f_i, g_i)$ . The matrices can then be derived from their Vandermonde matrix  $V$ , as shown below.

$$A^T = V_{n \times m}^T S_A \quad (7)$$

$$B^T = S_B V_{n \times n}^{-T} \quad (8)$$

$$G = S_G V_{n \times r} \quad (9)$$

where  $S_A$ ,  $S_B$ , and  $S_G$  are diagonal square matrices satisfying the following condition. For more details of derivation, please refer to [41].

$$S_A S_B S_G = I \quad (10)$$

#### 3.2. Group-wise quantization and optimized kernels

Naive application of model quantization to Winograd convolutions is often a challenging task, as shown in other studies [5, 10]. This is mainly because the quantization errors would exacerbate the numerical errors of Winograd convolution, especially for large tile sizes, thus usually leading to significant model accuracy degradations.

Inspired by the recent advances in LLM quantization, we adopt a fine-grained group-wise quantization scheme for both the weights and activations because of its reduced quantization errors and minimal dependence on the calibration data. Tensors are first divided into hardware vectorization-friendly groups, as illustrated in Figure 1, and each group is then quantized individually to reduce the impact of outliers and improve precision. We also apply this for the Winograd input transform (Eq. 4) and output transform (Eq. 6), resulting in a fully quantized Winograd convolution pipeline.

In addition, we develop a set of highly optimized matrix multiply kernels for group-wise quantized 8-bit diffusion models to unleash the full potential of modern CPUs. These kernels can fully take advantage of available vector and matrix multiply instructions to maximize MAC unit utilization, amortize the cost of loading the operands, minimize overhead and memory accesses, and achieve the best possible



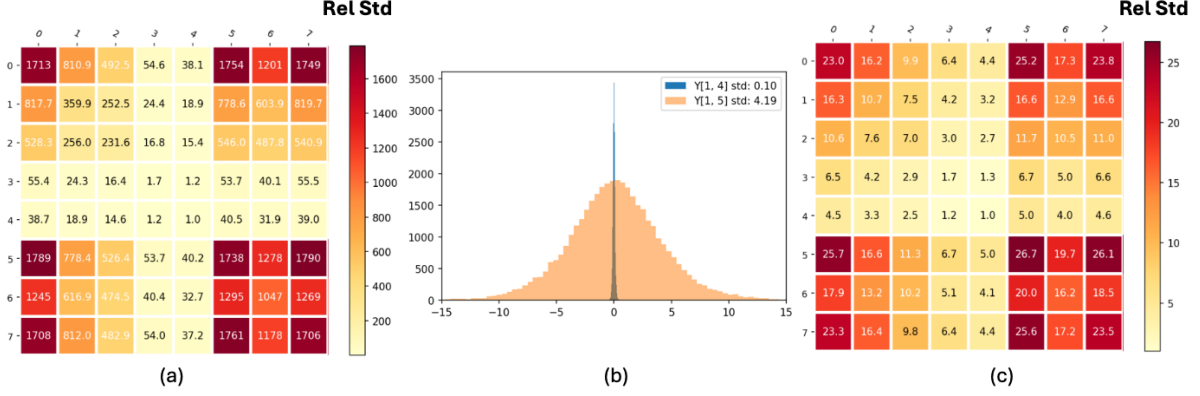


Figure 3. Dynamic ranges across different taps or pixels of the Winograd domain output ( $Y$ ) are very different. (a) Relative standard deviations at all of the  $8 \times 8$  locations of the Winograd domain output tile, obtained from the InstaFlow-0.9B model. (b) Histograms of values at locations (1, 4) and (1, 5). (c) Relative standard deviations after learning Winograd scales.

performance (to date) on CPUs for diffusion models. Our highly optimized group-wise quantized kernels can achieve similar runtime performance as that of the coarser-grained quantization methods while offering better quality.

## 4. Learnable scales for group-wise quantized Winograd convolution

### 4.1. Learnable Winograd transform scales

Because of the fine granularity of group-wise quantization, we observe that direct application of it to the Winograd input transform and Hadamard product computation generally would not have a significant impact on model quality. However, this is not the case for the output transform. This is mainly because of the huge dynamic range differences across different taps or pixels of the Winograd domain output,  $Y$  (Eq. 5), as shown in Figure 3(a). In order to utilize efficient integer arithmetic operations, there should be either a single scale factor for the entire output tile or one for each row or column. However, both would lead to significant quantization errors due to the ‘cross’-like dynamic range differences at the  $8 \times 8$  locations. Although pixel-wise quantization can effectively reduce this quantization error, it precludes the efficient use of integer computation kernels.

Given the fact that the output feature map  $Y$  in the Winograd domain depends on inputs, original pre-trained weights, and the input transformation ( $B$ ) and weight transformation ( $G$ ) matrices, the large dynamic range of  $Y$  across pixels is primarily attributed to the values of  $G$  and  $W$ , as well as the variances of values in weights and inputs. In the absence of finetuning original weights in the PTQ setup, the large range differences may be effectively reduced by manipulating the two transformation matrices,  $B$  and  $G$ , and in turn their norm of rows. From Eq. 8 and Eq. 9, each row of the Vandermonde matrices of  $B^T$  and  $G$  are scaled by the diagonal scaling matrices  $S_B$  and  $S_G$ , respectively, which

are directly controlling the norms of the row vectors in  $B^T$  and  $G$ .

Following this intuition, we propose to reduce the quantization noise of Winograd output transform by learning the diagonal scaling matrices  $S_B$  and  $S_G$ , while  $S_A = (S_B S_G)^{-1}$ , as given by Eq. 10, and can be easily computed. More formally, if we define the Vandermonde matrices as  $V_B = V_{n \times n}^{-T}$ ,  $V_G = V_{n \times r}$  and  $V_A = V_{n \times m}^T$  to simplify notation, then the Winograd transformations can be rewritten as:

$$W = S_G V_G w V_G^T S_G \quad (11)$$

$$X = S_B V_B x V_B^T S_B \quad (12)$$

$$y = V_A S_A Y S_A V_A^T \quad (13)$$

Then we apply group-wise quantization and integer matrix multiplication to all stages of Winograd convolution, specifically:

$$\begin{aligned} X &\approx s_{qB} s_{qB} s_{qx} Q\left(\frac{S_B V_B}{s_{qB}}\right) Q\left(\frac{x}{s_{qx}}\right) Q\left(\frac{V_B^T S_B}{s_{qB}}\right) \\ &= \tilde{X} \end{aligned} \quad (14)$$

$$Y \approx s_{qW} s_{qX} Q\left(\frac{W}{s_{qW}}\right) Q\left(\frac{\tilde{X}}{s_{qX}}\right) = \tilde{Y} \quad (15)$$

$$\begin{aligned} y &\approx s_{qA} s_{qA} s_{qY} Q\left(\frac{V_A S_A}{s_{qA}}\right) Q\left(\frac{\tilde{Y}}{s_{qY}}\right) Q\left(\frac{S_A V_A^T}{s_{qA}}\right) \\ &= \tilde{y} \end{aligned} \quad (16)$$

where  $s_{q*}$  are the group-wise quantization scaling factors for the weights, activations, intermediate results, and Winograd transformation matrices and  $Q$  is quantization function. We use simple min-max to dynamically quantize all activations during the forward pass.

## 4.2. Random Gaussian noise for fine-tuning scales

We then use gradient descent (SGD) to optimize the following objective and use the learned Winograd scale matrices  $S_G$  and  $S_B$  to determine the group-wise quantization scale factors,  $s_{q^*}$  in Eq. 14-16. For ease of setup, we treat each convolution layers independently. Unlike previous studies that use domain-specific data for QAT or finetuning, we instead only use random Gaussian or random uniform noise to learn the Winograd scaling matrices. In previous studies, the quantized model was calibrated and finetuned using a few samples from the training data, which might affect the quantized foundation diffusion models’ generalization to unknown cases and downstream tasks. In addition, rather than finetuning scale factors separately for each convolution layer of a diffusion model, we learn a single set of finetuned scale factors for all layers. This further enhances the generalizability of our method.

$$S_G^*, S_B^* = \arg \min_{S_G, S_B} \sum_{i \in D} \|y_i - \tilde{y}_i\| \quad (17)$$

## 5. Experiments

### 5.1. Experimental settings

In this section, we evaluate the proposed learnable Winograd scales method on two latent diffusion models, InstaFlow-0.9B [21] and Stable Diffusion [30], for text-to-image generation using the MS-COCO 2017 dataset [19], which contains 5000 images. We use pre-trained checkpoints with a image resolution of  $512 \times 512$ , and for stable diffusion, we follow the setup in [21] and choose the DPM-Solver++ [23] sampler with 25 time steps and the classifier-free guidance scale of 5.0. To further demonstrate the applicability of the proposed method, we also experiment with ResNets [11] on image classification task with the Imagenet [8] dataset.

We apply group-wise quantization to all linear and convolution layers of all components of the diffusion model pipeline, including the text encoder, UNet, and decoder. We also quantize the attention weights, attention query and key multiplication, and value multiplication, which are not often performed in previous studies [17]. Furthermore, we compare the effects of two autoencoder models, the original autoencoder in [30], denoted as AKL, and the tiny autoencoder [3], denoted as TAESD. To evaluate the quality of images generated, we followed the practices of previous works and computed FID [13] and CLIP [29] (ViT-g-14 model) scores using the torchmetrics package.

In the following, we first show results of applying only group-wise quantization and then the results of combining it with Winograd convolution using our proposed method.

---

### Algorithm 1 Data-free fully group-wise quantized Winograd transform by scales optimization

---

**Input:** Number of epochs  $N$ , number of batches per epoch  $B$ , number of convolution layers selected in each training iteration  $K$ , a collection of standard convolution layers with pre-trained weights  $C_1$ , a collection of corresponding group-wise quantized Winograd convolution layers  $C_2$ , and they all share a single set of learnable transformation scaling factors  $S_G, S_B$ .

**Output:** Learned scaling factors  $S_G, S_B$  for all layers in  $C_2$ .

```

1: for  $i = 1$  to  $N$  do
2:   for  $j = 1$  to  $B$  do
3:     Randomly pick  $K$  conv layers from  $C_1$ , e.g., 2
4:     Find the corresponding  $K$  Winograd conv layers from  $C_2$ 
5:     Generate random noise inputs, Gaussian or uniform,  $x_i$  for each pair of  $Conv2d_i, WinoConv2d_i$ 
6:     for  $k = 1$  to  $K$  do
7:        $y_i = Conv2d_i(x_i)$ 
8:        $\tilde{y}_i = WinoConv2d_i(x_i)$ 
9:       loss = SQNR( $y_i, \tilde{y}_i$ )
10:      loss.backward()
11:    end for
12:    optimizer.step()
13:  end for
14: end for

```

---

### 5.2. Text-to-image generation

Table 1 and table 2 show the results for the InstaFlow-0.9B model with AKL and TAESD, respectively. It can be seen that with a bit width of W8A8, group-wise quantization maintains the same level of image generation quality and text-image alignment as the original FP16 model. For TAESD, it even improved upon the baseline FP16 model in both metrics. Quantizing the weights to 4-bit leads to more distortion, but there is no significant degradation of image quality. When applying group-wise quantization to the standard Winograd convolution, FID and CLIP scores degrade drastically. Our method can restore most of the image generation quality for both  $F(4, 3)$  and  $F(6, 3)$  configurations.

Figure 4 and Figure 5 show some qualitative examples of the challenges of direct application of group-wise quantization to the Winograd pipeline, especially for TAESD where the images are completely destroyed. Because of this, we do not compute FID and CLIP scores for TAESD under this condition. As shown in Figure 3, this is mainly due to the huge dynamic range differences in the Winograd output  $Y$ . After applying the learned Winograd scales obtained from Algorithm 1, both images are mostly recovered. Figure 3(c) also shows the effectiveness of our method in dynamic range equalization in the Winograd output  $Y$ .

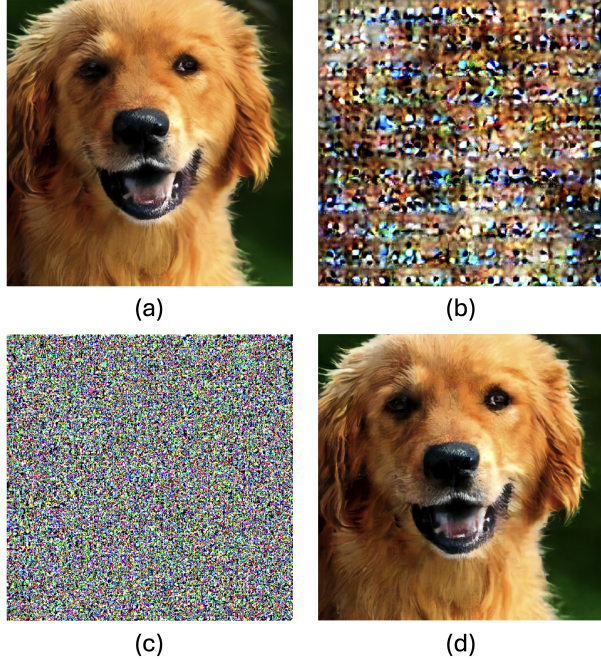


Figure 4. (a) Image generated from FP16 model with AKL. (b) (c) Images generated from W8A8 group-wise quantized standard Winograd convolution, using AKL and TAESD, respectively. (d) Image generated from W8A8 group-wise quantized Winograd convolution with learned scales and AKL. InstaFlow-0.9B model and Winograd F(6, 3) was used.

IF-0.9B, COCO2017-5k, AKL				
Model	tile size	Bits	FID(↓)	CLIP(↑)
FP16	N/A	16/16	23.00	30.19
W4A8	N/A	4/8	28.73	29.09
W8A8	N/A	8/8	23.04	30.16
W8A8 Winograd	F(4,3)	8/8	243.02	13.18
Standard scales	F(6,3)	8/8	326.96	5.95
W8A8 Winograd	F(4,3)	8/8	23.38	30.07
Learned scales	F(6,3)	8/8	27.05	29.58

Table 1. Results on the InstaFlow-0.9B model with group-wise quantization, Winograd convolution, and AKL autoencoder.

IF-0.9B, COCO2017-5k, TEASD				
Model	tile size	Bits	FID(↓)	CLIP(↑)
FP16	N/A	16/16	26.39	29.73
W4A8	N/A	4/8	31.94	28.80
W8A8	N/A	8/8	24.67	30.08
W8A8 Winograd	F(4,3)	8/8	N/A	N/A
Standard scales	F(6,3)	8/8	N/A	N/A
W8A8 Winograd	F(4,3)	8/8	28.19	29.57
Learned scales	F(6,3)	8/8	34.00	28.93

Table 2. Results on the InstaFlow-0.9B model with group-wise quantization, Winograd convolution, and TEASD autoencoder.

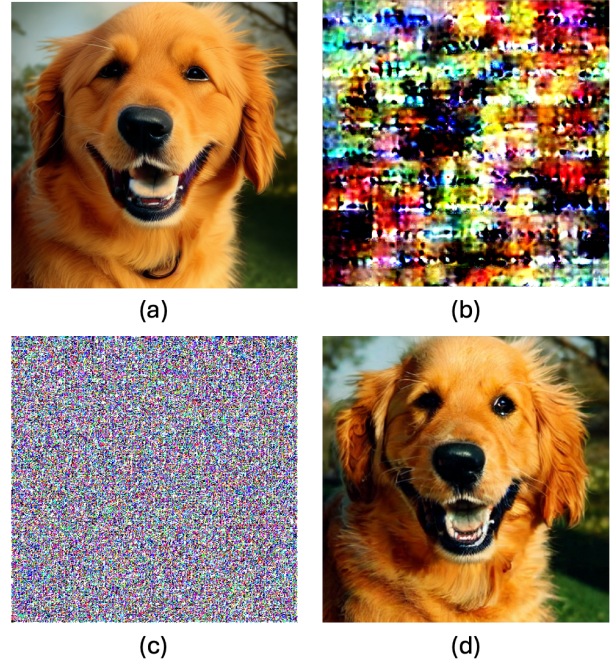


Figure 5. (a) Image generated from FP16 model with AKL. (b) (c) Images generated from W8A8 group-wise quantized standard Winograd convolution, using AKL and TAESD, respectively. (d) Image generated from W8A8 group-wise quantized Winograd convolution with learned scales and AKL. Stable Diffusion V1.5 model and Winograd F(6, 3) was used.

SD-1.5, COCO2017-5k, AKL				
Model	tile size	Bits	FID(↓)	CLIP(↑)
FP16	N/A	16/16	21.72	31.72
W4A8	N/A	4/8	20.62	31.16
W8A8	N/A	8/8	21.80	31.70
W8A8 Winograd	F(4,3)	8/8	261.84	12.66
Standard scales	F(6,3)	8/8	329.25	3.56
W8A8 Winograd	F(4,3)	8/8	22.29	31.70
Learned scales	F(6,3)	8/8	20.72	31.51

Table 3. Results on the Stable Diffusion V1.5 model with group-wise quantization, Winograd convolution, and AKL autoencoder.

SD-1.5, COCO2017-5k, TEASD				
Model	tile size	Bits	FID(↓)	CLIP(↑)
FP16	N/A	16/16	22.04	31.76
W4A8	N/A	4/8	21.78	31.12
W8A8	N/A	8/8	22.10	31.74
W8A8 Winograd	F(4,3)	8/8	N/A	N/A
Standard scales	F(6,3)	8/8	N/A	N/A
W8A8 Winograd	F(4,3)	8/8	22.10	31.66
Learned scales	F(6,3)	8/8	20.64	31.47

Table 4. Results on the Stable Diffusion V1.5 model with group-wise quantization, Winograd convolution, and TEASD autoencoder.



Model	tile size	Bits	Standard Winograd	BQW [6]	PAW+FSQ [5]	Winograd with Learned Scales
ResNet18	F(4,3)	W8/A8	4.26%	68.94%	68.16%	<b>69.44%</b>
	69.76%	F(6,3)	W8/A8	0.08%	66.08%	66.89%
ResNet34	F(4,3)	W8/A8	5.98%	72.86%	71.75%	<b>73.06%</b>
	73.30%	F(6,3)	W8/A8	0.18%	70.87%	69.72%
ResNet50	F(4,3)	W8/A8	56.84%	<b>76.10%</b>	73.84%	75.87%
	76.15%	F(6,3)	W8/A8	29.45%	<b>75.79%</b>	75.36%

Table 5. ResNets Top-1 accuracy results on the ImageNet dataset.

Table 3 and Table 4 show the evaluation results from Stable diffusion V1.5, using DPMSolver++ [23] sampler with 25 sampling steps and a classifier-free guidance scale of 5.0. Similar to InstaFlow-0.9B, we observe that group-wise quantization to W8A8 exhibited almost no degradation in image generation quality with either AKL or TEASD. Direct application of group-wise quantization to Winograd convolution also leads to almost complete loss of model quality, e.g., FID increases from 21.72 to 329.25, but this is reversed to the most extent by our method. It is worth noting that, while the bit-width setting of W4A8 and some Winograd cases showed improvements in FID when compared to the baseline FP16 model, we observe some distortions in some of the generated images when compared to the W8A8 quantization or the FP16 model. This may have to do with the unreliability of the FID metric in image quality evaluation, as mentioned in [14, 26, 37].

### 5.3. Image classification

The evaluation results from ResNets on the ImageNet are shown in Table 5. We compare it to two methods: BQW [6] and PAW+FSQ [5]. Similar to findings from the diffusion models, group-wise quantization of the standard Winograd convolution to W8A8 significantly degraded ResNets classification accuracy in both  $F(4, 3)$  and  $F(6, 3)$  configurations. After utilizing the learned Winograd transform scales, we recovered most of the accuracies of the original full-precision model. Furthermore, our method outperformed PAW+FSQ by 1.62% and 2.56% in top-1 ImageNet accuracy on ResNet-18 and ResNet-34, respectively, for Winograd  $F(6, 3)$ .

### 5.4. Runtime improvements

Finally, we measure the runtime improvement of convolution layers as well as the end-to-end runtime of the InstaFlow-0.9B diffusion model on Arm Graviton3 CPUs with varying thread counts (cores). We use the stable-diffusion.cpp [1] framework to collect the inference runtime. As evident from Figure 6(a), the highly optimized kernels offer a significant improvement in runtime for group-wise quantized convolution layers. The fully-quantized Winograd convolution provides an additional 31.3% relative improvement over the optimized standard convolution

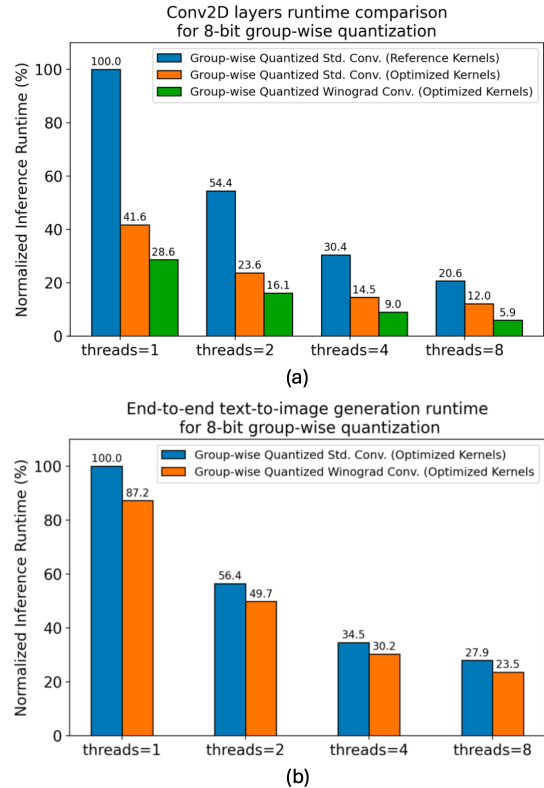


Figure 6. Convolution layers runtime improvements by using group-wise fully-quantized Winograd convolution.

layers. This translates into an 12.8% overall runtime improvement for the diffusion model for a single thread, as shown in Figure 6(b).

## 6. Conclusion

The exorbitant computational and storage overhead of large-scale diffusion models limit their practicality for on-device inference. We present a novel, lightweight method that (1) employs group-wise PTQ on both weights and activations, and (2) fully quantizes fast Winograd convolution by fine-tuning only the scale parameters of the transformation matrices, all without requiring any calibration data. Our method, implemented using highly optimized CPU kernels, maintains image generation quality and offers nearly

full-precision image classification accuracy while significantly speeding up CPU wall-clock time for large-scale diffusion models.

## References

- [1] stable-diffusion.cpp. 8
- [2] Syed Asad Alam, Andrew Anderson, Barbara Barabasz, and David Gregg. Winograd convolution for deep neural networks: Efficient point selection, 2022. 11
- [3] Ollin Boer Bohan. Tiny autoencoder for stable diffusion. 6
- [4] Lei Chen, Yuan Meng, Chen Tang, Xinzhu Ma, Jingyan Jiang, Xin Wang, Zhi Wang, and Wenwu Zhu. Q-dit: Accurate post-training quantization for diffusion transformers. *CoRR*, abs/2406.17343, 2024. 1, 3
- [5] Tianqi Chen, Weixiang Xu, Weihan Chen, Peisong Wang, and Jian Cheng. Towards efficient and accurate winograd convolution via full quantization. In *Advances in Neural Information Processing Systems*, 2023. 2, 3, 4, 8
- [6] Vladimir Chikin and Vladimir Kryzhanovskiy. Channel balancing for accurate quantization of winograd convolutions. In *2022 IEEE/CVF Conference on Computer Vision and Pattern Recognition (CVPR)*, 2022. 2, 3, 8, 11
- [7] Steve Dai, Rangha Venkatesan, Mark Ren, Brian Zimmer, William Dally, and Brucek Khailany. Vs-quant: Per-vector scaled quantization for accurate low-precision neural network inference. In *Proceedings of Machine Learning and Systems*, pages 873–884, 2021. 2
- [8] Jia Deng, Wei Dong, Richard Socher, Li-Jia Li, Kai Li, and Li Fei-Fei. Imagenet: A large-scale hierarchical image database. In *2009 IEEE Conference on Computer Vision and Pattern Recognition*, 2009. 6
- [9] Prafulla Dhariwal and Alexander Nichol. Diffusion models beat gans on image synthesis. In *Advances in Neural Information Processing Systems*, pages 8780–8794, 2021. 1
- [10] Javier Fernandez-Marques, Paul Whatmough, Andrew Mundy, and Matthew Mattina. Searching for winograd-aware quantized networks. *Proceedings of Machine Learning and Systems*, 2020. 2, 3, 4, 12, 13
- [11] Kaiming He, Xiangyu Zhang, Shaoqing Ren, and Jian Sun. Deep residual learning for image recognition. In *Proceedings of the IEEE Conference on Computer Vision and Pattern Recognition (CVPR)*, 2016. 6
- [12] Yefei He, Luping Liu, Jing Liu, Weijia Wu, Hong Zhou, and Bohan Zhuang. Ptqd: Accurate post-training quantization for diffusion models. In *Advances in Neural Information Processing Systems*, 2023. 1, 3
- [13] Martin Heusel, Hubert Ramsauer, Thomas Unterthiner, Bernhard Nessler, and Sepp Hochreiter. Gans trained by a two time-scale update rule converge to a local nash equilibrium. In *Advances in Neural Information Processing Systems*, 2017. 6
- [14] Sadeep Jayasumana, Srikumar Ramalingam, Andreas Veit, Daniel Glasner, Ayan Chakrabarti, and Sanjiv Kumar. Re-thinking fid: Towards a better evaluation metric for image generation. In *Proceedings of the IEEE/CVF Conference on Computer Vision and Pattern Recognition (CVPR)*, 2024. 8
- [15] Andrew Lavin and Scott Gray. Fast algorithms for convolutional neural networks. In *Proceedings of the IEEE Conference on Computer Vision and Pattern Recognition (CVPR)*, 2016. 2, 3, 4, 11
- [16] Guangli Li, Zhen Jia, Xiaobing Feng, and Yida Wang. Lowino: Towards efficient low-precision winograd convolutions on modern cpus. In *Proceedings of the 50th International Conference on Parallel Processing*, 2021. 3
- [17] Xiuyu Li, Yijiang Liu, Long Lian, Huanrui Yang, Zhen Dong, Daniel Kang, Shanghang Zhang, and Kurt Keutzer. Q-diffusion: Quantizing diffusion models. In *Proceedings of the IEEE/CVF International Conference on Computer Vision (ICCV)*, 2023. 1, 3, 6, 12, 13
- [18] Yuhang Li, Ruihao Gong, Xu Tan, Yang Yang, Peng Hu, Qi Zhang, Fengwei Yu, Wei Wang, and Shi Gu. {BRECQ}: Pushing the limit of post-training quantization by block reconstruction. In *International Conference on Learning Representations*, 2021. 3
- [19] Tsung-Yi Lin, Michael Maire, Serge Belongie, Lubomir Bourdev, Ross Girshick, James Hays, Pietro Perona, Deva Ramanan, C. Lawrence Zitnick, and Piotr Dollár. Microsoft coco: Common objects in context, 2015. 6
- [20] Luping Liu, Yi Ren, Zhijie Lin, and Zhou Zhao. Pseudo numerical methods for diffusion models on manifolds, 2022. 12
- [21] Xingchao Liu, Xiwen Zhang, Jianzhu Ma, Jian Peng, and qiang liu. InstafLOW: One step is enough for high-quality diffusion-based text-to-image generation. In *The Twelfth International Conference on Learning Representations*, 2024. 3, 6
- [22] Cheng Lu, Yuhao Zhou, Fan Bao, Jianfei Chen, Chongxuan LI, and Jun Zhu. Dpm-solver: A fast ode solver for diffusion probabilistic model sampling in around 10 steps. In *Advances in Neural Information Processing Systems*, 2022. 3
- [23] Cheng Lu, Yuhao Zhou, Fan Bao, Jianfei Chen, Chongxuan Li, and Jun Zhu. Dpm-solver++: Fast solver for guided sampling of diffusion probabilistic models, 2023. 6, 8, 12
- [24] Eric Luhman and Troy Luhman. Knowledge distillation in iterative generative models for improved sampling speed, 2021. 3
- [25] Lingchuan Meng and John Brothers. Efficient winograd convolution via integer arithmetic. *CoRR*, abs/1901.01965, 2019. 2, 3
- [26] Muhammad Ferjad Naeem, Seong Joon Oh, Youngjung Uh, Yunjey Choi, and Jaeyun Yoo. Reliable fidelity and diversity metrics for generative models. In *Proceedings of the 37th International Conference on Machine Learning*. PMLR, 2020. 8
- [27] Markus Nagel, Rana Ali Amjad, Mart Van Baalen, Christos Louizos, and Tijmen Blankevoort. Up or down? Adaptive rounding for post-training quantization. In *Proceedings of the 37th International Conference on Machine Learning*. PMLR, 2020. 3
- [28] Dustin Podell, Zion English, Kyle Lacey, Andreas Blattmann, Tim Dockhorn, Jonas Müller, Joe Penna, and Robin Rombach. SDXL: Improving latent diffusion models



- for high-resolution image synthesis. In *The Twelfth International Conference on Learning Representations*, 2024. 1
- [29] Alec Radford, Jong Wook Kim, Chris Hallacy, Aditya Ramesh, Gabriel Goh, Sandhini Agarwal, Girish Sastry, Amanda Askell, Pamela Mishkin, Jack Clark, Gretchen Krueger, and Ilya Sutskever. Learning transferable visual models from natural language supervision. In *Proceedings of the 38th International Conference on Machine Learning*. PMLR, 2021. 6
- [30] Robin Rombach, Andreas Blattmann, Dominik Lorenz, Patrick Esser, and Björn Ommer. High-resolution image synthesis with latent diffusion models. In *Proceedings of the IEEE/CVF Conference on Computer Vision and Pattern Recognition (CVPR)*, 2022. 1, 6, 12
- [31] Chitwan Saharia, William Chan, Saurabh Saxena, Lala Li, Jay Whang, Emily L Denton, Kamyar Ghasemipour, Raphael Gontijo Lopes, Burcu Karagol Ayan, Tim Salimans, Jonathan Ho, David J Fleet, and Mohammad Norouzi. Photorealistic text-to-image diffusion models with deep language understanding. In *Advances in Neural Information Processing Systems*, 2022. 1, 3
- [32] Tim Salimans and Jonathan Ho. Progressive distillation for fast sampling of diffusion models. In *International Conference on Learning Representations*, 2022. 3
- [33] Yuzhang Shang, Zhihang Yuan, Bin Xie, Bingzhe Wu, and Yan Yan. Post-training quantization on diffusion models. In *Proceedings of the IEEE/CVF Conference on Computer Vision and Pattern Recognition (CVPR)*, 2023. 1, 3
- [34] Junhyuk So, Jungwon Lee, Daehyun Ahn, Hyungjun Kim, and Eunhyeok Park. Temporal dynamic quantization for diffusion models. In *Thirty-seventh Conference on Neural Information Processing Systems*, 2023. 3
- [35] Jiaming Song, Chenlin Meng, and Stefano Ermon. Denoising diffusion implicit models. In *International Conference on Learning Representations*, 2021. 1, 3
- [36] Yang Song, Jascha Sohl-Dickstein, Diederik P Kingma, Abhishek Kumar, Stefano Ermon, and Ben Poole. Score-based generative modeling through stochastic differential equations. In *International Conference on Learning Representations*, 2021. 3
- [37] George Stein, Jesse Cresswell, Rasa Hosseinzadeh, Yi Sui, Brendan Ross, Valentin Vilecroze, Zhaoyan Liu, Anthony L Caterini, Eric Taylor, and Gabriel Loaiza-Ganem. Exposing flaws of generative model evaluation metrics and their unfair treatment of diffusion models. In *Advances in Neural Information Processing Systems*, 2023. 8
- [38] Yang Sui, Yanyu Li, Anil Kag, Yerlan Idelbayev, Junli Cao, Ju Hu, Dhritiman Sagar, Bo Yuan, Sergey Tulyakov, and Jian Ren. Bitsfusion: 1.99 bits weight quantization of diffusion model. In *The Thirty-eighth Annual Conference on Neural Information Processing Systems*, 2024. 1
- [39] Siao Tang, Xin Wang, Hong Chen, Chaoyu Guan, Zewen Wu, Yansong Tang, and Wenwu Zhu. Post-training quantization for text-to-image diffusion models with progressive calibration and activation relaxing, 2024. 1, 3
- [40] Siao Tang, Xin Wang, Hong Chen, Chaoyu Guan, Zewen Wu, Yansong Tang, and Wenwu Zhu. Post-training quantization with progressive calibration and activation relaxing for text-to-image diffusion models. In *Computer Vision – ECCV 2024: 18th European Conference, Milan, Italy, September 29–October 4, 2024, Proceedings, Part LVI*, 2024. 3
- [41] Kevin Vincent, Kevin Stephano, Michael A. Frumkin, Boris Ginsburg, and Julien Demouth. On improving the numerical stability of winograd convolutions. In *5th International Conference on Learning Representations, ICLR 2017, Toulon, France, April 24-26, 2017, Workshop Track Proceedings*. OpenReview.net, 2017. 4, 11
- [42] Changyuan Wang, Ziwei Wang, Xiuwei Xu, Yansong Tang, Jie Zhou, and Jiwen Lu. Towards accurate post-training quantization for diffusion models. In *Proceedings of the IEEE/CVF Conference on Computer Vision and Pattern Recognition (CVPR)*, 2024. 1, 3
- [43] Haoxuan Wang, Yuzhang Shang, Zhihang Yuan, Junyi Wu, Junchi Yan, and Yan Yan. Quest: Low-bit diffusion model quantization via efficient selective finetuning, 2024. 1, 3
- [44] Shmuel Winograd. *Arithmetic complexity of computations*. Siam, 1980. 3
- [45] Tianwei Yin, Michaël Gharbi, Richard Zhang, Eli Shechtman, Frédo Durand, William T. Freeman, and Taesung Park. One-step diffusion with distribution matching distillation. In *Proceedings of the IEEE/CVF Conference on Computer Vision and Pattern Recognition (CVPR)*, 2024. 3
- [46] Tianchen Zhao, Xuefei Ning, Tongcheng Fang, Enshu Liu, Guyue Huang, Zinan Lin, Shengen Yan, Guohao Dai, and Yu Wang. Mixdq: Memory-efficient few-step text-to-image diffusion models with metric-decoupled mixed precision quantization, 2024. 1, 3

# Data-Free Group-Wise Fully Quantized Winograd Convolution via Learnable Scales

## Supplementary Material

### 7. Winograd transformations for convolution

#### 7.1. Standard Winograd transforms

Following [41], given a set of polynomial points  $(f_i, g_i)$ , the Vandermonde matrix  $V_{a \times b}$  is constructed as below,

$$\begin{bmatrix} f_0^0 g_0^{b-1} & f_0^1 g_0^{b-2} & \cdots & f_0^{b-1} g_0^0 \\ f_1^0 g_1^{b-1} & f_1^1 g_1^{b-2} & \cdots & f_1^{b-1} g_1^0 \\ \vdots & \vdots & \ddots & \vdots \\ f_{a-1}^0 g_{a-1}^{b-1} & f_{a-1}^1 g_{a-1}^{b-2} & \cdots & f_{a-1}^{b-1} g_{a-1}^0 \end{bmatrix} \quad (18)$$

For standard Winograd convolution, we adopt the widely used polynomial points and scaling factors, as mentioned in [2, 6, 15, 41]. Specifically, for  $F(4, 3)$  the polynomial points, scaling factors, Vandermonde and transformation matrices are the following,

$$\begin{aligned} (f_i, g_i) &= [(0, 1), (1, 1), (-1, 1), \\ &\quad (2, 1), (-2, 1), (1, 0)] \\ S_A &= [1, 1, 1, 1, 1, 1] \end{aligned} \quad (19)$$

$$\begin{aligned} S_B &= [4, -6, -6, 24, 24, 1] \\ S_G &= [1/4, -1/6, -1/6, 1/24, 1/24, 1] \end{aligned}$$

$$V_{6 \times 4} = \begin{bmatrix} 1 & 0 & 0 & 0 \\ 1 & 1 & 1 & 1 \\ 1 & -1 & 1 & -1 \\ 1 & 2 & 4 & 8 \\ 1 & -2 & 4 & -8 \\ 0 & 0 & 0 & 1 \end{bmatrix} \quad (20)$$

$$V_{6 \times 6}^{-T} = \begin{bmatrix} 1 & 0 & -5/4 & 0 & 1/4 & 0 \\ 0 & 2/3 & 2/3 & -1/6 & -1/6 & 0 \\ 0 & -2/3 & 2/3 & 1/6 & -1/6 & 0 \\ 0 & -1/12 & -1/24 & 1/12 & 1/24 & 0 \\ 0 & 1/12 & -1/24 & -1/12 & 1/24 & 0 \\ 0 & 4 & 0 & -5 & 0 & 1 \end{bmatrix} \quad (21)$$

$$V_{6 \times 3} = \begin{bmatrix} 1 & 0 & 0 \\ 1 & 1 & 1 \\ 1 & -1 & 1 \\ 1 & 2 & 4 \\ 1 & -2 & 4 \\ 0 & 0 & 1 \end{bmatrix} \quad (22)$$

$$\begin{aligned} A^T &= V_{6 \times 4}^T \text{diag}(S_A) \\ &= \begin{bmatrix} 1 & 1 & 1 & 1 & 1 & 0 \\ 0 & 1 & -1 & 2 & -2 & 0 \\ 0 & 1 & 1 & 4 & 4 & 0 \\ 0 & 1 & -1 & 8 & -8 & 1 \end{bmatrix} \end{aligned} \quad (23)$$

$$\begin{aligned} B^T &= \text{diag}(S_B) V_{6 \times 6}^{-T} \\ &= \begin{bmatrix} 4 & 0 & -5 & 0 & 1 & 0 \\ 0 & -4 & -4 & 1 & 1 & 0 \\ 0 & 4 & -4 & -1 & 1 & 0 \\ 0 & -2 & -1 & 2 & 1 & 0 \\ 0 & 2 & -1 & -2 & 1 & 0 \\ 0 & 4 & 0 & -5 & 0 & 1 \end{bmatrix} \end{aligned} \quad (24)$$

$$\begin{aligned} G &= \text{diag}(S_G) V_{6 \times 3} \\ &= \begin{bmatrix} 1/4 & 0 & 0 \\ -1/6 & -1/6 & -1/6 \\ -1/6 & 1/6 & -1/6 \\ 1/24 & 1/12 & 1/6 \\ 1/24 & -1/12 & 1/6 \\ 0 & 0 & 1 \end{bmatrix} \end{aligned} \quad (25)$$

For  $F(6, 3)$ , the polynomial points, scaling factors, Vandermonde and transformation matrices are the following,

$$\begin{aligned} (f_i, g_i) &= [(0, 1), (1, 1), (-1, 1), (2, 1), \\ &\quad (-2, 1), (1/2, 1), (-1/2, 1), (1, 0)] \\ S_A &= [1, 1, 1, 1, 1, 1, 1, 1] \\ S_B &= [1, -9/2, -9/2, 90, 90, 45/32, 45/32, 1] \\ S_G &= [1, -2/9, -2/9, 1/90, 1/90, 32/45, 32/45, 1] \end{aligned} \quad (26)$$

$$V_{8 \times 6} = \begin{bmatrix} 1 & 0 & 0 & 0 & 0 & 0 \\ 1 & 1 & 1 & 1 & 1 & 0 \\ 1 & -1 & 1 & -1 & 1 & -1 \\ 1 & 2 & 4 & 8 & 16 & 32 \\ 1 & -2 & 4 & -8 & 16 & -32 \\ 1 & 1/2 & 1/4 & 1/8 & 1/16 & 1/32 \\ 1 & -1/2 & 1/4 & -1/8 & 1/16 & -1/32 \\ 0 & 0 & 0 & 0 & 0 & 1 \end{bmatrix} \quad (27)$$

$$V_{8 \times 8}^{-T} = \begin{bmatrix} 1 & 0 & -21/4 & 0 & 21/4 & 0 & -1 & 0 \\ 0 & -2/9 & -2/9 & 17/18 & 17/18 & -2/9 & -2/9 & 0 \\ 0 & 2/9 & -2/9 & -17/18 & -17/18 & 2/9 & -2/9 & 0 \\ 0 & 1/180 & 1/360 & -1/36 & -1/72 & 1/45 & 1/90 & 0 \\ 0 & -1/180 & 1/360 & 1/36 & -1/72 & -1/45 & 1/90 & 0 \\ 0 & 64/45 & 128/45 & -16/9 & -32/9 & 16/45 & 32/45 & 0 \\ 0 & -64/45 & 128/45 & 16/9 & -32/9 & -16/45 & 32/45 & 0 \\ 0 & -1/4 & 0 & 21/4 & 0 & -21/4 & 0 & 1 \end{bmatrix} \quad (28)$$

$$V_{8 \times 3} = \begin{bmatrix} 1 & 0 & 0 \\ 1 & 1 & 1 \\ 1 & -1 & 1 \\ 1 & 2 & 4 \\ 1 & -2 & 4 \\ 1 & 1/2 & 1/4 \\ 1 & -1/2 & 1/4 \\ 0 & 0 & 1 \end{bmatrix} \quad (29)$$

$$A^T = V_{8 \times 6}^T \text{diag}(S_A) = \begin{bmatrix} 1 & 1 & 1 & 1 & 1 & 1 & 1 & 0 \\ 0 & 1 & -1 & 2 & -2 & 1/2 & -1/2 & 0 \\ 0 & 1 & 1 & 4 & 4 & 1/4 & 1/4 & 0 \\ 0 & 1 & -1 & 8 & -8 & 1/8 & -1/8 & 0 \\ 0 & 1 & 1 & 16 & 16 & 1/16 & 1/16 & 0 \\ 0 & 1 & 1 & 32 & -32 & 1/32 & -1/32 & 0 \end{bmatrix} \quad (30)$$

$$B^T = \text{diag}(S_B) V_{8 \times 8}^{-T} = \begin{bmatrix} 4 & 0 & -21 & 0 & 21 & 0 & -4 & 0 \\ 0 & 4 & 4 & -17 & -17 & 4 & 4 & 0 \\ 0 & -4 & 4 & 17 & -17 & -4 & 4 & 0 \\ 0 & 2 & 1 & -10 & -5 & 8 & 4 & 0 \\ 0 & -2 & 1 & 10 & -5 & -8 & 4 & 0 \\ 0 & 8 & 16 & -10 & -20 & 2 & 4 & 0 \\ 0 & -8 & 16 & 10 & -20 & -2 & 4 & 0 \\ 0 & -4 & 0 & 21 & 0 & -21 & 0 & 4 \end{bmatrix} /4 \quad (31)$$

$$G = \text{diag}(S_G) V_{6 \times 3} = \begin{bmatrix} 1 & 0 & 0 \\ -2/9 & -2/9 & 2/9 \\ -2/9 & 2/9 & 2/9 \\ 1/90 & 1/45 & -2/45 \\ 1/90 & -1/45 & 2/45 \\ 32/45 & 16/45 & 8/45 \\ 32/45 & -16/45 & 8/45 \\ 0 & 0 & 1 \end{bmatrix} \quad (32)$$

## 7.2. Learned Winograd scales

Table 6 shows the difference in values between the standard Winograd scales and our learned Winograd scales for  $F(6, 3)$ . It is worth noting that the magnitudes of  $S_A$  have become smaller while those of  $S_G$  are bigger, and  $S_B$  stays relatively unchanged.

## 8. Comparison with learning transformation matrices instead of Winograd scales

[10] proposed to treat the Winograd transformation matrices  $A$ ,  $B$ , and  $G$  as learnable parameters and jointly optimize them with other model weights and biases in a QAT setup. Although this is much less practical in the domain of Generative AI, as mentioned above, we still adopt this paradigm to

tile size	Standard Winograd scales			Learned Winograd scales		
	$S_A$	$S_B$	$S_G$	$S_A$	$S_B$	$S_G$
$F(6, 3)$	1	1	1	0.525	-1.378	-1.382
	1	-4.5	-0.222	0.354	-4.908	-0.576
	1	-4.5	-0.222	0.351	-4.912	-0.579
	1	90	0.0111	0.0601	90.366	0.184
	1	90	0.0111	0.0609	90.362	0.182
	1	1.406	0.711	0.491	1.820	1.119
	1	1.406	0.711	0.490	1.823	1.120
	1	1	1	0.519	1.386	1.391

Table 6. Comparison between standard Winograd scales and our learned Winograd scales.

IF-0.9B, COCO2017-5k, AKL				
Model	tile size	Bits	FID(↓)	CLIP(↑)
FP16	N/A	16/16	23.00	30.19
W4A8	N/A	4/8	28.73	29.09
W8A8	N/A	8/8	23.04	30.16
W8A8 Winograd	F(4,3)	8/8	243.02	13.18
Standard scales	F(6,3)	8/8	326.96	5.95
W8A8 Winograd	F(4,3)	8/8	23.38	30.07
Learned scales	F(6,3)	8/8	27.05	29.58
W8A8 Winograd	F(4,3)	8/8	228.18	15.17
Learned transforms	F(6,3)	8/8	360.14	7.46

Table 7. Results on the InstaFlow-0.9B model with group-wise quantization, Winograd convolution, and AKL autoencoder. Comparison between learning scales and learning transformation matrices.

compare with our method. All training setups are the same except that transformation matrices  $A$ ,  $B$ , and  $G$  are learned directly using random noise inputs instead of learning only the scaling factors  $S_A$ ,  $S_B$ , and  $S_G$ . The results are shown in Table 7 using the InstaFlow-0.9B model with AKL autoencoder. It can be seen that learning the transformation matrices directly offers almost no improvement compared to the standard Winograd transforms. This could be due to the use of random noise as layer inputs and treating each layer independently.

## 9. Comparison of group-wise quantization against other quantization methods

Table 8 and Table 9 show the comparison between our group-wise quantization method against a popular, recently proposed quantization scheme, called Q-Diffusion[17], for Stable Diffusion V1.4[30] with DPMSolver++[23] and PLMS[20] sampler, respectively. All models were sampled for 25 steps, and MSCOCO 2017 was used to generate FID and CLIP scores. We conducted the experiments with Q-Diffusion using the official codebase and pre-calibrated quantized checkpoints released by the authors.

SD-1.4, COCO2017-5k, AKL, DPMSolver++				
Model	tile size	Bits	FID(↓)	CLIP(↑)
FP16	N/A	16/16	21.63	31.72
W4A8	N/A	4/8	21.21	30.84
W8A8	N/A	8/8	21.52	31.70
W8A8	N/A	8/8	21.03	31.16
Q-Diffusion [17]	N/A	8/8	21.03	31.16

Table 8. Results on the Stable Diffusion V1.4 model for group-wise quantization, Winograd convolution, AKL autoencoder and DPMSolver++ sampler with 25 steps. Comparison with the results from Q-Diffusion [17].

SD-1.4, COCO2017-5k, AKL, PLMS				
Model	tile size	Bits	FID(↓)	CLIP(↑)
FP16	N/A	16/16	22.94	31.74
W4A8	N/A	4/8	22.19	30.01
W8A8	N/A	8/8	22.48	31.68
W8A8	N/A	8/8	24.42	31.07
Q-Diffusion [17]	N/A	8/8	24.42	31.07

Table 9. Results on the Stable Diffusion V1.4 model for group-wise quantization, Winograd convolution, AKL autoencoder and PLMS sampler with 25 steps. Comparison with the results from Q-Diffusion [17].

Figure 7, 8, 9, 10, 11, and 12 compare more qualitative examples generated by the 8-bit Winograd convolution with those generated by the full-precision, 4-bit, and 8-bit models with standard convolution. We also show the images generated by 8-bit Q-diffusion using standard convolution. It can be observed that W8A8 group-wise quantized Stable Diffusion can generate images of nearly identical quality compared with either the FP16 or Q-Diffusion model while being calibration-free. For W4A8, group-wise quantization shows no significant drop in image generation quality and text image alignment.

## 10. Transferability of learned Winograd scales across datasets

Because Winograd scales are learned from random noise inputs in our method, the same Winograd scale used for one dataset should scale to other datasets also. Data-free finetuning makes Winograd scale values transferable across datasets. Table 10 shows the accuracy results for the CIFAR10 dataset, whereas the same learned Winograd scale values used for the ImageNet dataset previously are applied to another dataset, the CIFAR10 dataset in this case. Winograd, using learned scales, can successfully restore the accuracy of the full-precision ResNet network for both tile sizes. This confirms the transferability of our learned Winograd scales across datasets.

Model	tile size	Bits	Standard Winograd	Winograd with Learned Scales
ResNet18	F(4,3)	W8/A8	92.55%	93.00%
	93.07%	F(6,3)	W8/A8	33.62%
ResNet34	F(4,3)	W8/A8	93.05%	93.26%
	93.33%	F(6,3)	W8/A8	22.90%
ResNet50	F(4,3)	W8/A8	93.49%	93.70%
	93.65%	F(6,3)	W8/A8	81.13%

Table 10. ResNets Top-1 accuracy results on the CIFAR-10 dataset.

## 11. Comparison to prior QAT works for fully quantizing Winograd

In comparison to previous QAT studies [10] that achieve full quantization by learning Winograd transformation matrices, we can achieve comparable results by fine-tuning only the Winograd scales. As shown in Table 10, 8-bit ResNet18 with Winograd achieves an accuracy of 93% for  $F(4, 3)$  (an accuracy drop of 0.07% in comparison to the full-precision model) using our learned scales, whereas Winograd-aware QAT [10] observes an accuracy drop of 0.7% for the similar setting.



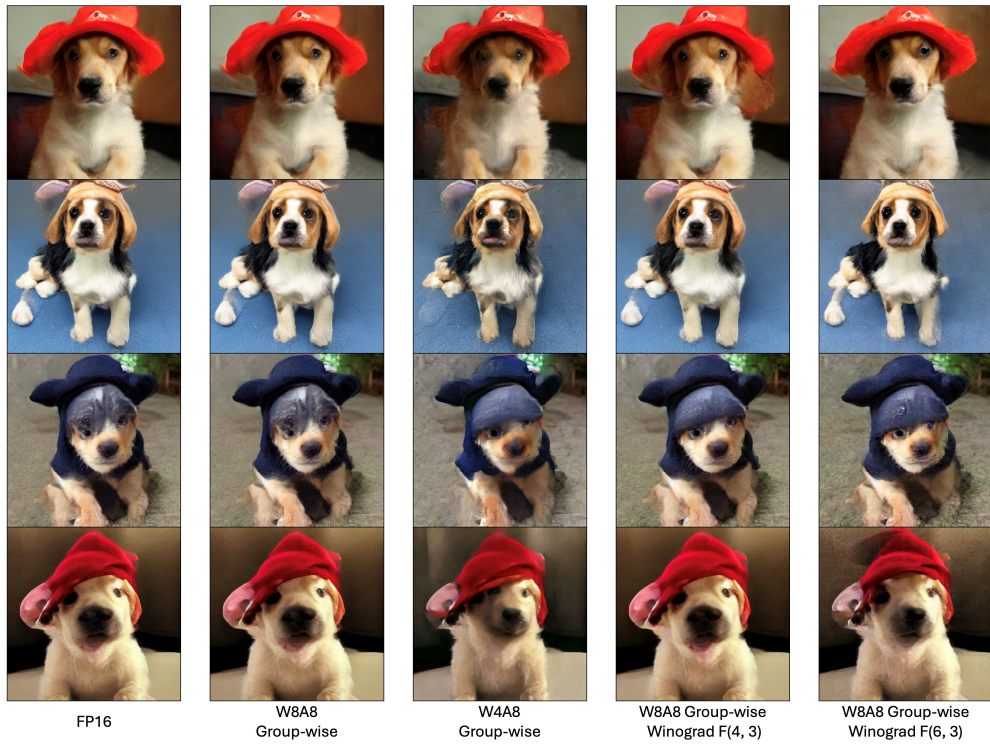


Figure 7. InstaFlow-0.9B with AKL. Prompt "A puppy wearing a hat; realistic"



Figure 8. InstaFlow-0.9B with AKL. Prompt "A shiny motorcycle on the field; realistic, high-resolution"



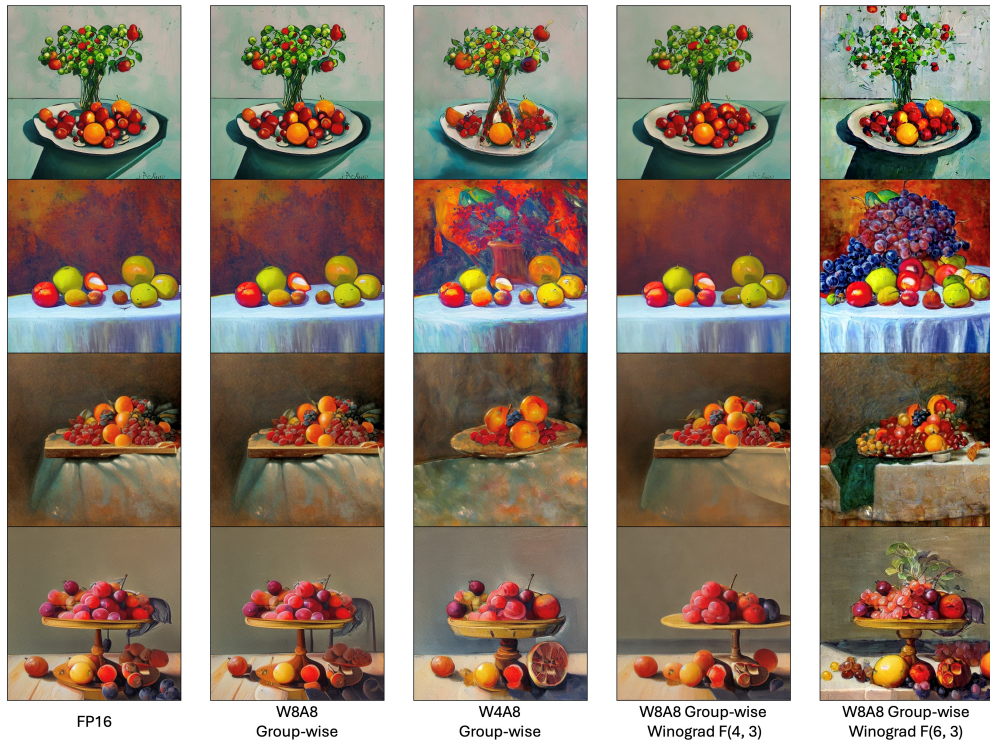


Figure 9. Stable Diffusion V1.5 with AKL and DPMSolver++ sampler. Prompt "A painting of a table with fruit on top of it"



Figure 10. Stable Diffusion V1.5 with AKL and DPMSolver++ sampler. Prompt "A realistic photo of a lovely cat"



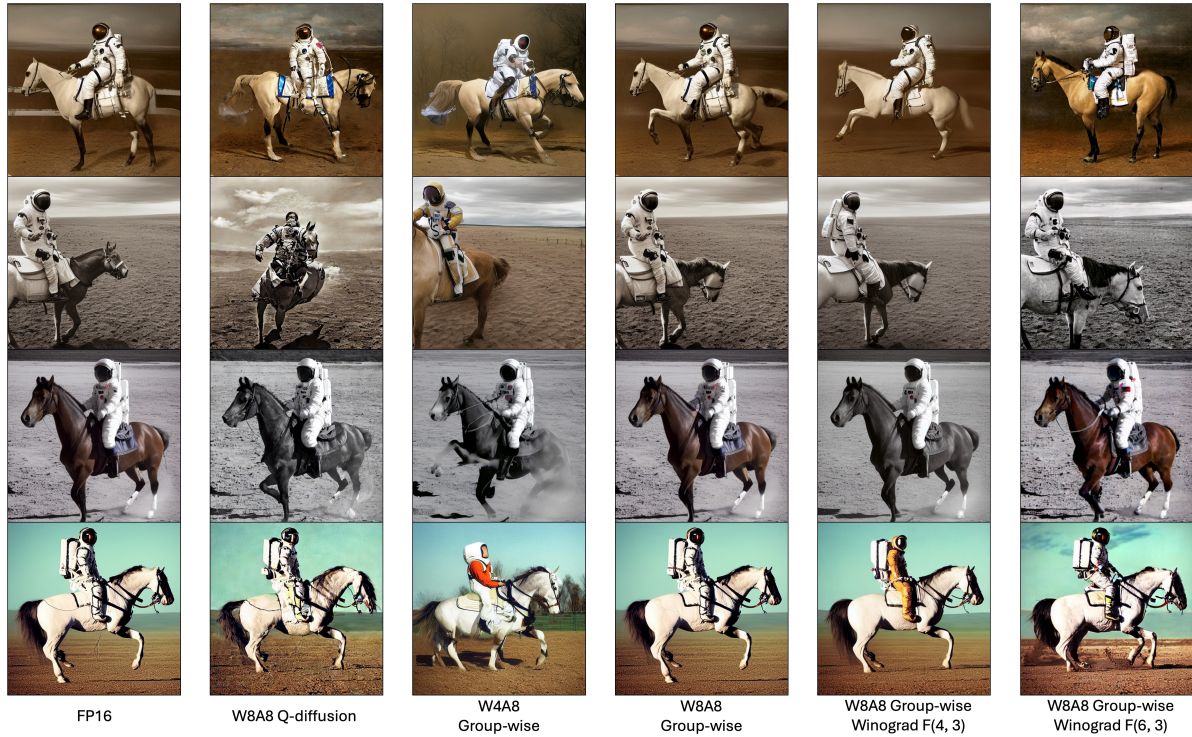


Figure 11. Stable Diffusion V1.4 with AKL and DPMSolver++ sampler. Prompt "A photograph of an astronaut riding a horse"



Figure 12. Stable Diffusion V1.4 with AKL and DPMSolver++ sampler. Comparison with Q-Diffusion. Prompt "A building wall and pair of doors, along with vases of flowers on the outside of the building"